Construction of Organic Heterojunctions as Metal-Free Photocatalysts for Enhancing Water Splitting and Phenol Degradation by Regulating Charge Flow

Yang You[#[a]], Xiaoyu Shi[#[a]], Liang Huang[a], Jie Zhao [a], Wen Ji[a], Libo Li[b], Donglei Bu*[a], and Shaoming Huang*[c]

[a] School of Materials and Energy, Guangzhou Key Laboratory of Low-Dimensional Materials and Energy Storage Devices, Guangdong University of Technology, Guangzhou 510006, P. R. China

[b] School of Chemistry and Chemical Engineering, Guangdong Prov Key Lab Green Chem Prod Technol, South China University of Technology, Guangzhou 510640, PR China

[c] School of Chemistry and Materials Science, Hangzhou Institute for Advanced Study University of Chinese Academy of Sciences, Hangzhou, 310024, P. R. China

[#]These authors contribute equally.

[*]Corresponding authors

E-mail: budonglei@gdut.edu.cn, smhuang@gdut.edu.cn

Materials and Methods

Materials:

3,4,9,10- perylenetetracarboxylic dianhydride, urea, imidazole, zinc acetate, 2,4,6-triformylphloroglucinol, 4,4" diamino-p-terphenyl, mesitylene, 1,4-dioxane, glacial acetic acid, and ethanol were used as received.

Synthesis of Catalysts:

Synthesis of perylene diimide polyme (UP): A mixture of 2.0 mmol of 3,4,9,10-perylenetetracarboxylic dianhydride (PTCDA), 2.2 mmol of urea, 5.0 g of imidazole, and 2.0 mmol of zinc acetate was heated at 150 ° C for 5 h with continuous stirring. Then, the mixture was poured into 100 mL ethanol and stirred for 15 min. The precipitate was collected through vacuum filtration and washed with distilled water three times. And the final perylene diimide polymer (PDIP) sample was then washed several times with DMSO until the washings became colorless to remove the short oligomers from the mixture and dried at 80 °Covernight.

Synthesis of TP-COF: A Pyrex tube was charged with 2,4,6-triformylphloroglucinol (21 mg, 0.1 mmol), 4,4" diamino-p-terphenyl (39 mg, 0.15 mmol), mesitylene (2 mL), 1,4-dioxane (4 mL), and aqueous acetic acid (0.2 mL, 6 M). This mixture was homogenized by sonication for 10 minutes and the tube was then flash frozen at 77 K (liquid N_2 bath) and degassed by three freeze-pump-thaw cycles, before evacuating to an internal pressure of 100 mTorr. The tube was then sealed off and heated at 150 °C for 3 days. The yellow precipitate was collected by centrifugation

and washed with anhydrous acetone (200 mL). After drying at 120 °C

Synthesis of UP@TP-COF-x: A Pyrex tube was charged with Tp (63 mg, 0.3 mmol), DT (117 mg, 0.45 mmol) and UPDI, where in different weight ratios of TP-COF/UPDI hybrid materials ranging from 0 to 40% (referred to TP-COF proportion) were synthesized and named TP-COF, UP@TP-COF-0.1, UP@TP-COF-0.2, UP@TP-COF-0.3, and UP@TP-COF-0.4, respectively. The above mixture was evenly dispersed in a solution containing mesitylene (1.5 mL), 1,2-dichlorobenzene (1.5 mL) and aqueous acetic acid (0.5 mL, 6 M) by sonicated for 30 min. Afterwards, the vacuum valve was flash frozen in a liquid N2 bath (77 K) and degassed by three freeze- pump-thaw cycles, sealed under vacuum, and then heated at 150 °C for 3 days. The yellow precipitate was collected by centrifugation and washed with anhydrous acetone (100 mL), and then dried at 90 °C for 12 h under vacuum to afford different weight ratios of TP-COF/UPDI hybrid materials photocatalysts.

General Methods:

X-ray diffraction (XRD) measurements were carried out on a Rigaku Smartlab 9kW X-ray diffractometer. Scanning electron microscope (SEM) characterization was carried out on a Thermo Fisher Apero C scanning electron microscope. Atomic force microscopy (AFM) measurements were carried out on a Multimode 8 AFM (Bruker, SO#47233). X-ray photoelectron spectroscopy (XPS) characterization was carried out on a Thermo Fisher Escalab 250Xi X-ray photoelectron spectrometer. Electron paramagnetic resonance (EPR) measurements were performed on a Bruker A300

electron paramagnetic resonance instrument. The Ultraviolet–visible diffuse reflectance spectra were measured by a UV-vis spectrophotometer (Shimadzu UV-3600), and $BaSO_4$ was used as a reflectance standard material and the scanning range was 200-900 nm. The Fourier transform infrared spectra (FT-IR) of the samples were analyzed by infrared spectrometer (Nicolet IS50 Thermo fisher) using KBr disk. The Photo-luminescence (PL) spectrum was performed using a Fuorolog-3 fluorescence lifetime spectrophotometer. Solid-state 13C CP/MAS NMR spectra were recordedbyusing a contact time of 3 ms on a Bruker AM-400 NMR spectrometer, equipped with a 5.0mm chemagnetics probe.

All of the photoelectrochemical measurements were measured on a CHI 760E electrochemical station (Shanghai Chenhua, China) in ambient conditions. Generally, 3 mg of photocatalyst were dispersed in 1 mL 1% nafion ethanol solution. A glassy carbon electrode with a photocatalyst deposited served as the working electrode, while a platinum sheet and an Ag/AgCl electrode served as the counter and reference electrode, respectively. The electrolyte was a 0.2 M Na_2SO_4 solution and a 300 W Xe lamp was used as the visible light source.

Photocatalytic Hydrogen and Oxygen Evolution

The time-dependent photocatalytic hydrogen production experiments were performed in Labsolar-6A online system (Beijing Perfectlight) at 5 ºC. A Xenon arc lamp (300 W) was employed as light source to trigger the photocatalytic reaction. The photocatalyst was dispersed in deionized water with sacrificial reagent in the reaction

cell by using a magnetic stirrer. Prior to the reaction, the mixture was degassed under vacuum to remove air. The generated gas phase products were characterized by Agilent 8860 gas chromatography (a molecular sieve 5A column, two Hayesep Q column, a thermal conductivity detector, a flame ionization detector, argon was used as carrier gas) connected with Perfectlight 6A system.

Photocatalytic Phenol Degradation Experiments

The catalysts were dispersed in a 10 mg/L phenol solution and stirred magnetically for 1 h under dark conditions to reach adsorption-desorption equilibrium. A 300 W xenon lamp was used as the light source, and a 420 nm cutoff filter was used to remove light at wavelengths not relevant to the environment. During the illumination process, 2 ml of the solution was removed at intervals and immediately centrifuged and filtered, and the supernatant was analyzed by high performance liquid chromatography (HPLC), and the remaining phenol content in the system was quantified by external standard method. The phenol concentration was determined using high-performance liquid chromatography (HPLC) (ACQUITY UPLC H-Class) equipped with an analytical column C18 and a detector (ACQUITY UPLC PDA) at 270 nm.

Computational Details

In Density Functional Theory (DFT) calculations, in order to avoid weak interactions between images, cluster model of Covalent Organic Framework (COF) was constructed in a 50×50×50 $Å^3$ box. Structural optimizations were performed by Vienna *Ab-initio* Simulation Package (VASP)[1] with the projector augmented wave (PAW)

method.[2] The exchange-functional was treated using the Perdew-Burke-Ernzerhof (PBE)[3] functional, in combination with the DFT-D3 correction.[4] Cut-off energy of the plane-wave basis was set as 450 eV. For optimization of geometry of COF, the Brillouin zone integration was performed with Gamma[5] *k*-point sampling of 1×1×1. The self-consistent calculations applied a convergence energy threshold of 10^{-5} eV. The equilibrium geometries and lattice constants were optimized with maximum stress on each atom within 0.02 eV $Å^{-1}$. Spin polarization method was adopted to describe magnetism brought by intermediates.

In calculation of Gibbs free energy, we built the adsorption model by employing the computational hydrogen electrode (CHE) model developed by Nørskov et al.[6]

Elementary steps of hydrogen evolution reaction (HER) were described as:

$$* + H^+ + e^- \rightarrow *H$$

$$*H + H^+ + e^- \rightarrow * + H_2(g)$$

Elementary steps of oxygen evolution reaction (OER) were described as single site and dual site pathway. Single site pathway were described as:

$$* + H_2O(l) \rightarrow *OH + H^+ + e^-$$

$$*OH \rightarrow *O + H^+ + e^-$$

$$*O + H_2O(l) \rightarrow *OOH + H^+ + e^-$$

$$*OOH \rightarrow * + O_2(aq) + H^+ + e^-$$

Dual site pathway were described as:

$$* + H_2O(l) \rightarrow *OH + H^+ + e^-$$

$$*OH \rightarrow *O + H^+ + e^-$$

$$*O + H_2O(l) \rightarrow *O\text{-}OH + H^+ + e^-$$

$$*O\text{-}OH \rightarrow *O\text{-}O + H^+ + e^-$$

$$*O\text{-}O \rightarrow * + O_2(aq)$$

* represents the bare surface of cluster model of COF. *i represent the surface of COF adsorbing intermediates i. Gibbs free energy of *i were calculated as G = E + G(T) + 0.0592pH - eU. E represents the total energy of COF. G(T) represents the thermal correction of Gibbs free energy of *i. Kelvin temperature T was set at 298.15K. Besides, pH was set at 3 and 7 to simulate acidic and neutral medium for HER and OER. The applied potentials U was set at 0V. Gibbs free energy of OH^- and O_2 in their aqueous phase were obtained based on standard molar free energy of formation and standard hydrogen electrode (SHE).[7] G(T) of *i were obtained by vaspkit interface.[8]

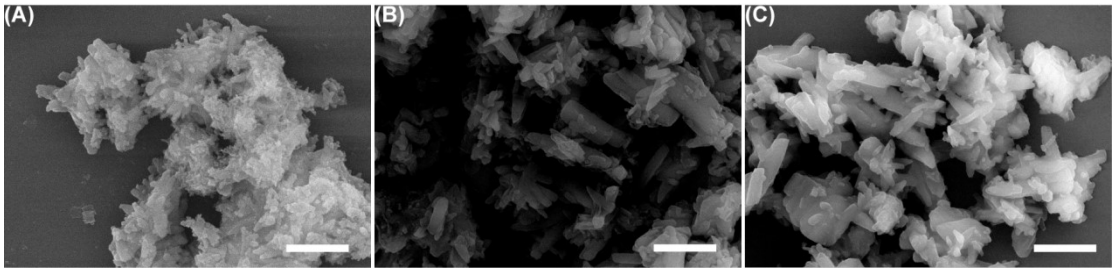

Figure S1. (A-C) SEM images of UP@TP-COF-0.1, UP@TP-COF-0.3, and UP@TP-COF-0.4, respectively. Scale bar = 2 μm.

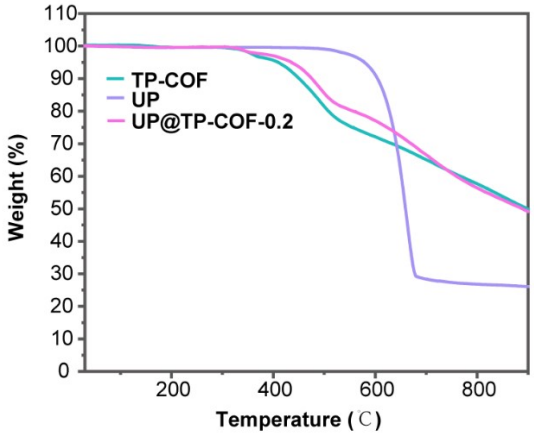

Figure S2. TGA of UP, TP-COF and UP@TP-COF-0.2.

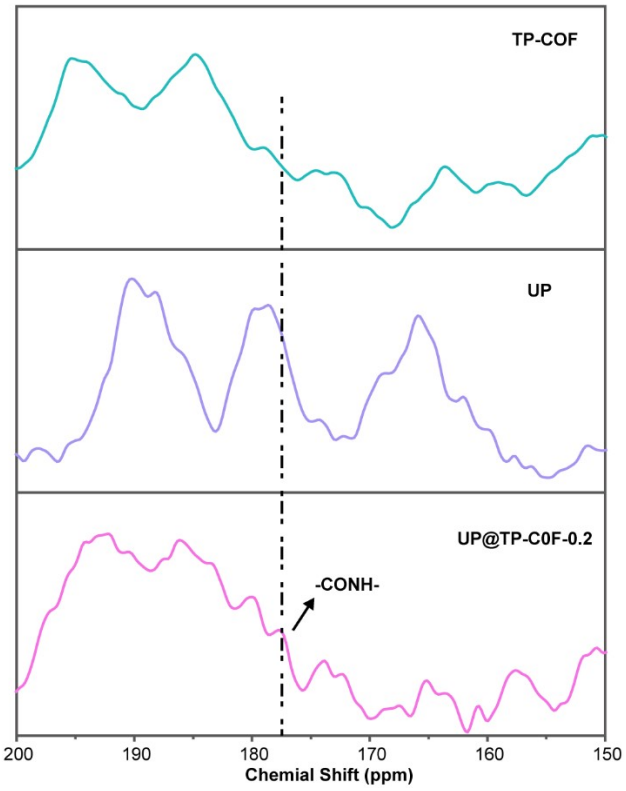

Figure S3. Solid state ^{13}C NMR of UP, TP-COF and UP@TP-COF-0.2.

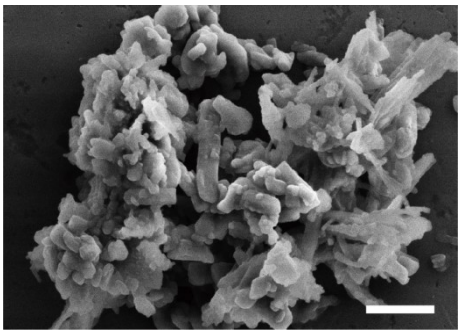

Figure S4. SEM image of the physically mixed UP and TP-COF. Scale bar = 4 μm.

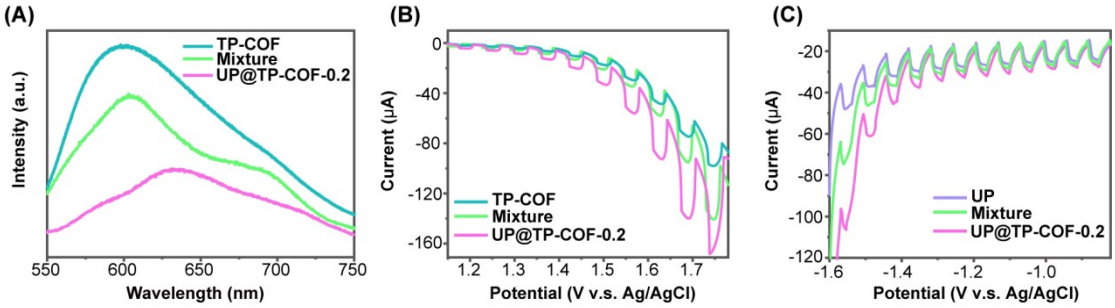

Figure S5. (A) PL spectra of TP-COF, UP@TP-COF-0.2, and the physical mixture. (B) LSV taken under chopped light of TP-COF, UP@TP-COF-0.2, and the physical mixture with positive bias. (C) LSV taken under chopped light of UP, UP@TP-COF-0.2, and the physical mixture with negative bias.

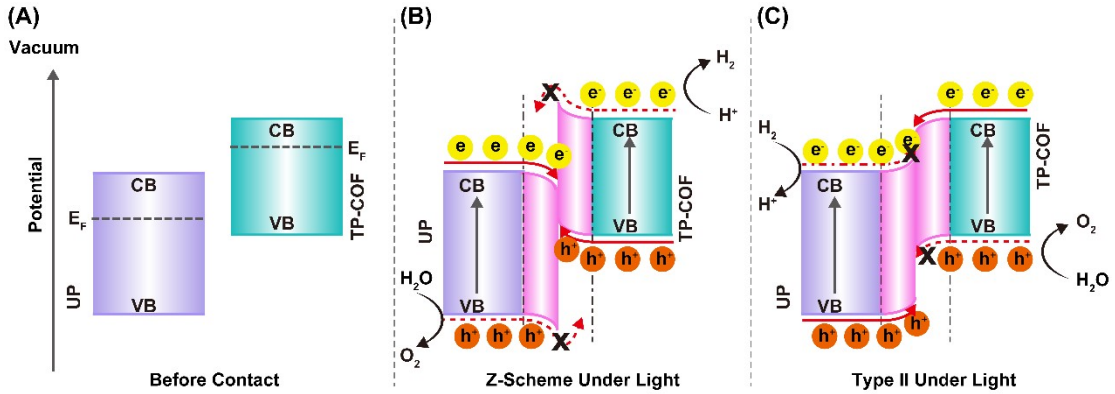

Figure S6. Schematic diagram of (A) band alignment of UP and TP-COF before contact, (B) charge transfer of Z-scheme mechanism and (C) charge transfer of type II mechanism, respectively.

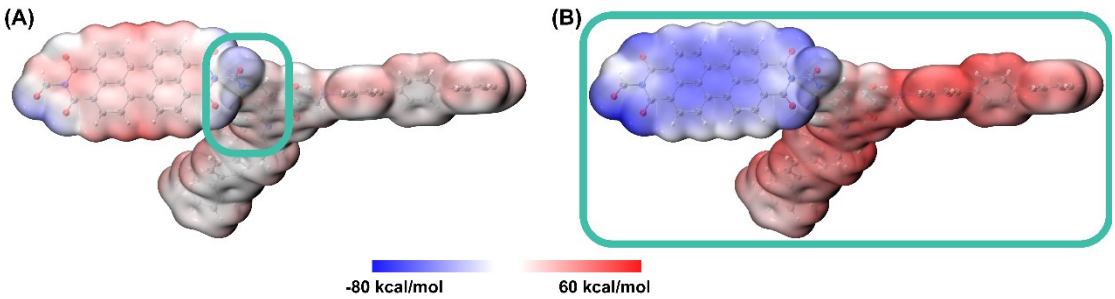

Figure S7. Calculated electron potential distribution (A) in dark and (B) under light, respectively. The green frames label the region of the IEF at the interface.

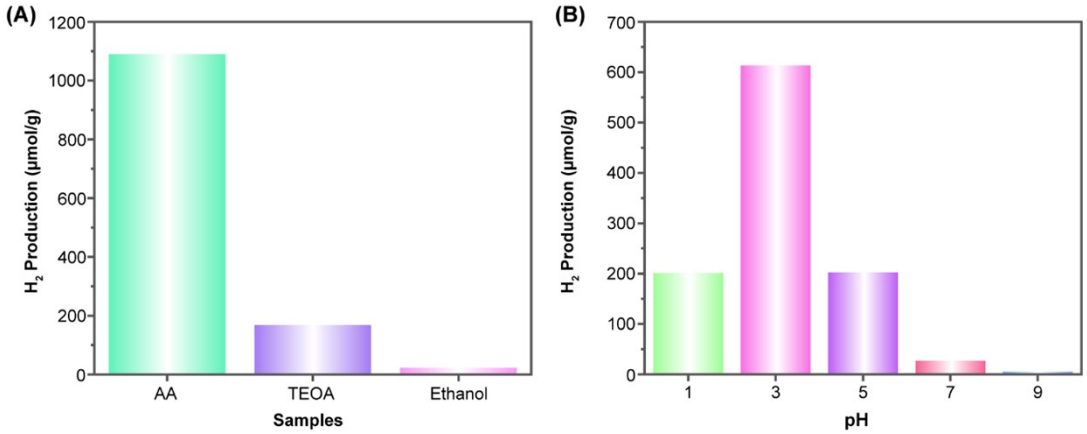

Figure S8. (A) Photocatalytic H_2 productivity of UP@TP-COF-0.2 with different sacrificing reagent (10 vol%) at pH = 3 and (B) Photocatalytic HER performance of UP@TP-COF-0.2 at different pH.

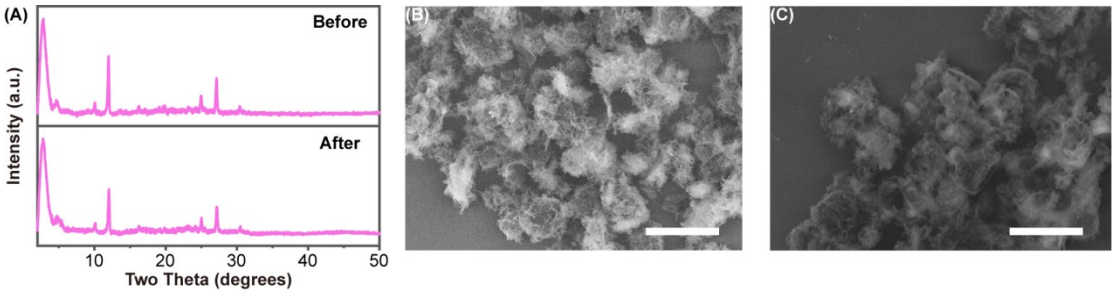

Figure S9. (A) PXRD of UP@TP-COF-0.2 before and after photocatalysis. (B) and (C) SEM images of UP@TP-COF-0.2 before and after photocatalysis, respectively.

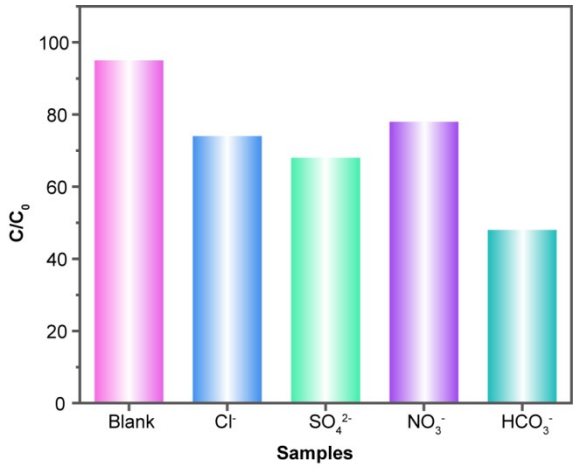

Figure S10. (A) Phenol degradation in water with different ions and (B) the rate constant (k) obtained by the fitted with first-order kinetics equation using the data in (A) of TP-COF, UP, UP@TP-COF-x, and the physical mixture, respectively.

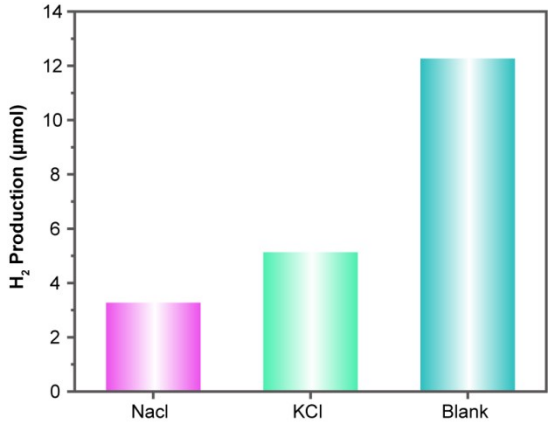

Figure S11. Photocatalytic hydrogen evolution rate of UP@TP-COF-0.2 in water with Na^+.

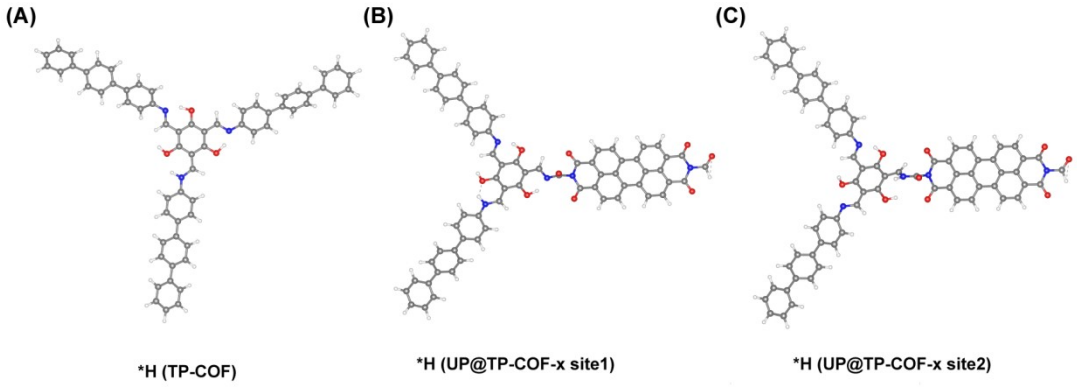

Figure S12. (A), (B) and (C) calculated structure of *H adsorption on TP-COF, site 1 and site 2 of UP@TP-COF-x, respectively.

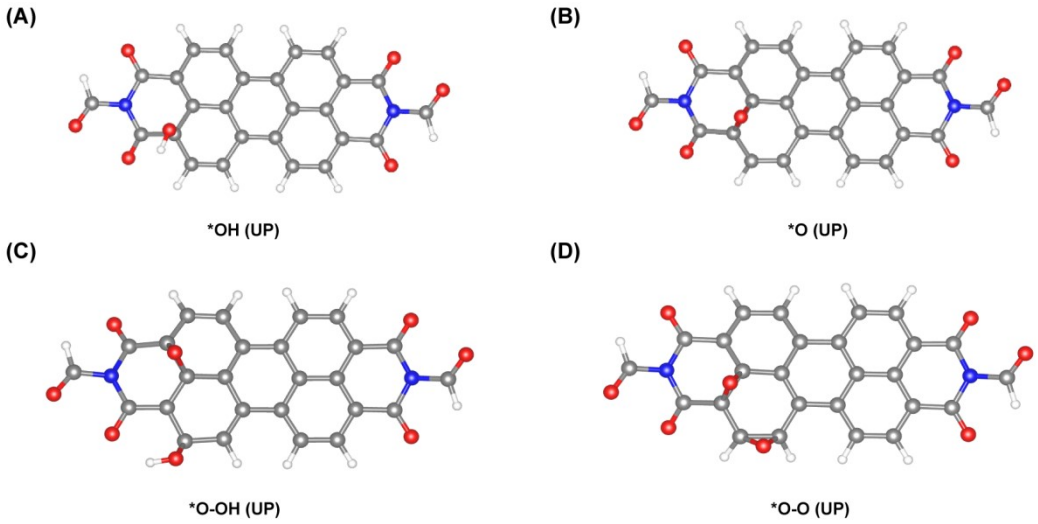

Figure S13. (A), (B) 9C) calculated structure of *H adsorption on TP-COF, site 1 and site 2 of UP@TP-COF-x, respectively.

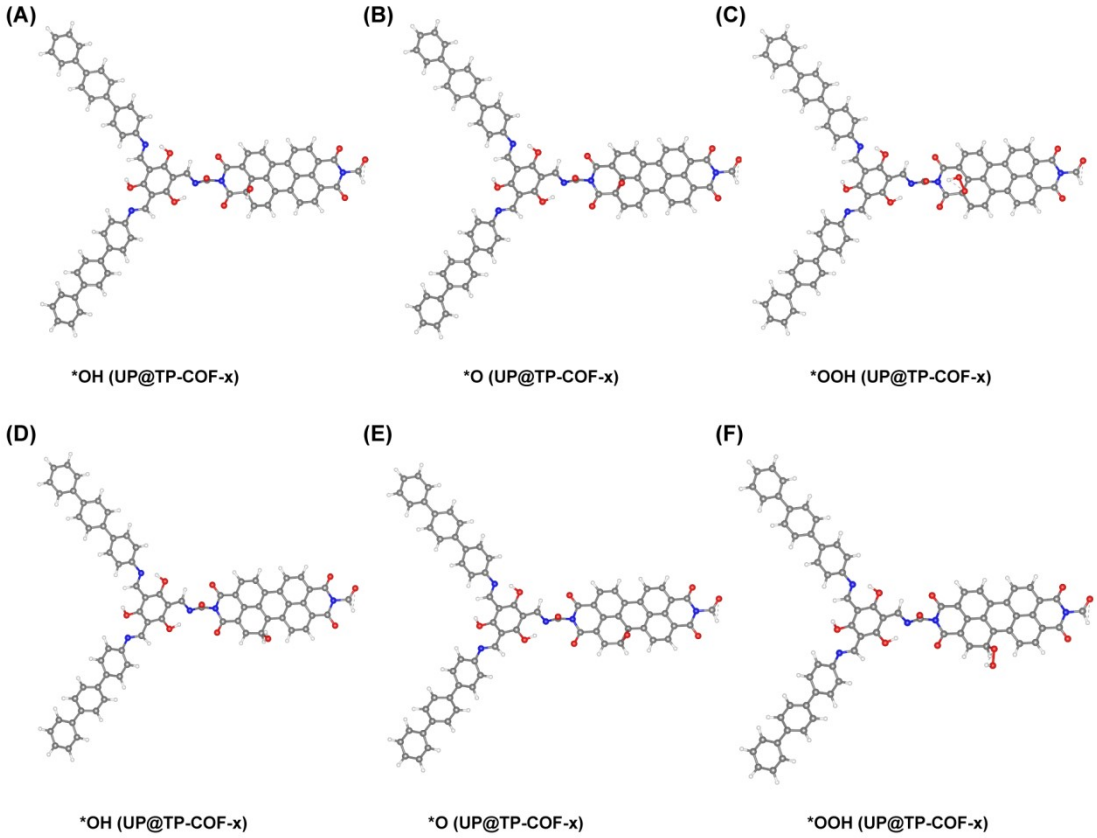

Figure S14. Calculated structures of OER intermediates adsorbed on UP@TP-COF-x of different sites via a single site pathway. (A) *OH, (B) *O and, (C) *OOH on site 1, respectively. (D) *OH, (E) *O and, (F) *OOH on site 2, respectively.

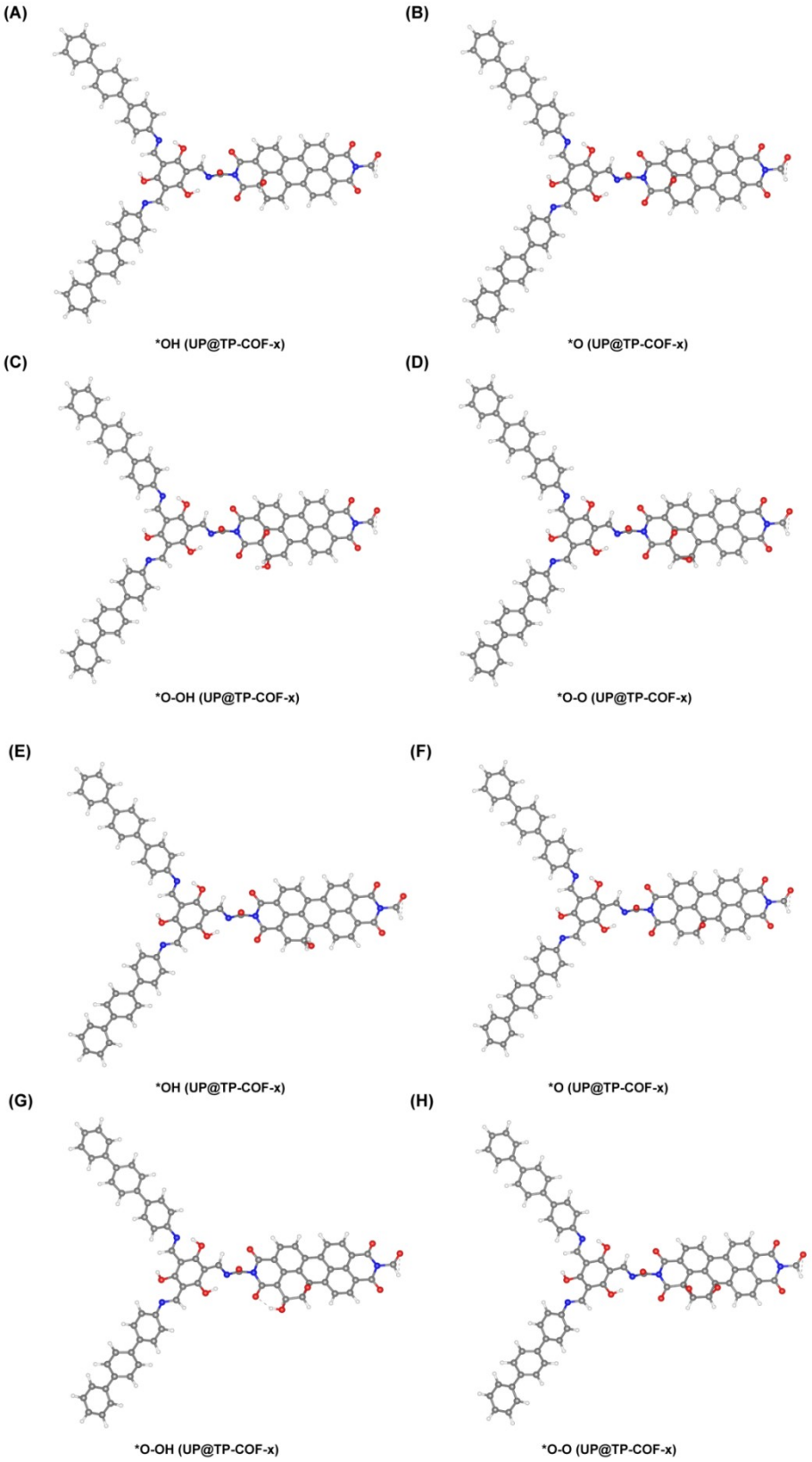

Figure S15. Calculated structures of OER intermediates adsorbed on UP@TP-COF-x of different sites via a double site pathway. (A) *OH, (B) *O, (C) *O-OH, and (D)

*O-O on site 1, respectively. (E) *OH, (F) *O, (G) *O-OH, and (H) *O-O on site 2, respectively.

Table S1. Comparison of HER Performance of Recently Reported Mental-Free Photocatalysts

Catalysts	H_2 evolution (μmol/gh)	Ref
UP@TP-COF-0.2	613.3	This work
TFPT-COF	312.5	[9]
CNF-4	352.2	[10]
PCN	30	[11]
Py-CITP-BT-COF	2200	[12]
PTP-COF	83	[13]
BP/RP-QD	441	[14]
TP-BDDA-COF	350	[15]
sp^2c-CMP	140	[16]
TTI-COF	460	[17]
A-TEBPY-COF	98	[18]
g-$C_{18}N_3$-COF	292	[19]
TpPa-COF-NO_2	220	[20]

Table S2. Comparison of OER Performance of Recently Reported Mental-Free Photocatalysts

Catalysts	O_2 evolution (μmol/gh)	Ref
UP@TP-COF-0.2	1169	This work
CTF-1	140	[21]
CTF-T1	17	[22]
CTF-0	60	[23]
PDI	3220	[24]
p-g-C_3N_4	46	[25]
S doped g-C_3N_4 (CNS)	42	[26]
nano-PDI	28	[27]
g-C_3N_4	12	[25]
PI	39	[28]
CTP-2	20	[29]

References:

1. J. Hafner, *J. Comput. Chem.*, 2008, **29**, 2044-2078.
2. P. E. Blöchl, *Phys. Rev. B*, 1994, **50**, 17953-17979.
3. K. B. John P. Perdew, * Matthias Ernzerhof, *Phys. Rev. Lett.*, 1996, **77**.
4. S. Grimme, *J. Comput. Chem.*, 2006, **27**, 1787-1799.
5. H. J. Monkhorst and J. D. Pack, *Phys. Rev. B*, 1976, **13**, 5188-5192.
6. a. G. S. K. Egill Skulason, a Jan Rossmeisl,a Thomas Bligaard,ab and a. H. J. c. a. J. K. N. Jeff Greeley, *Chem. Phys.*, 2007, DOI: 10.1039/b700099e, 3241-3250.
7. P. D. W. M. Haynes, 2016.
8. Vei Wang a, Nan Xu b, Jin-Cheng Liu c, Gang Tang d, Wen-Tong Geng, *Comput. Phys. Commun.*, 2021, **267**.

9. L. Stegbauer, K. Schwinghammer and B. V. Lotsch, *Chem. Sci.*, 2014, **5**, 2789-2793.

10. H. Wang, Y. Wu, M. Feng, W. Tu, T. Xiao, T. Xiong, H. Ang, X. Yuan and J. W. Chew, *Water Res.*, 2018, **144**, 215-225.

11. F. Xue, Y. Si, M. Wang, M. Liu and L. Guo, *Nano Energy*, 2019, **62**, 823-831.

12. W. Chen, L. Wang, D. Mo, F. He, Z. Wen, X. Wu, H. Xu and L. Chen, *Angew. Chem. Int. Ed.*, 2020, **59**, 16902-16909.

13. F. Haase, T. Banerjee, G. Savasci, C. Ochsenfeld and B. V. Lotsch, *Faraday Discuss.*, 2017, **201**, 247-264.

14. R. Shi, F. Liu, Z. Wang, Y. Weng and Y. Chen, *Chem. Commun.*, 2019, **55**, 12531-12534.

15. P. Pachfule, A. Acharjya, J. Roeser, T. Langenhahn, M. Schwarze, R. Schomäcker, A. Thomas and J. Schmidt, *J. Am. Chem. Soc.*, 2018, **140**, 1423-1427.

16. E. Jin, Z. Lan, Q. Jiang, K. Geng, G. Li, X. Wang and D. Jiang, *Chem*, 2019, **5**, 1632-1647.

17. Y. Yang, N. Luo, S. Lin, H. Yao and Y. Cai, *ACS Catal.*, 2022, **12**, 10718-10726.

18. L. Stegbauer, S. Zech, G. Savasci, T. Banerjee, F. Podjaski, K. Schwinghammer, C. Ochsenfeld and B. V. Lotsch, *Adv. Energy Mater.*, 2018, **8**, 1703278.

19. S. Wei, F. Zhang, W. Zhang, P. Qiang, K. Yu, X. Fu, D. Wu, S. Bi and F. Zhang, *J. Am. Chem. Soc.*, 2019, **141**, 14272-14279.

20. J. L. Sheng, H. Dong, X. B. Meng, H. L. Tang, Y. H. Yao, D. Q. Liu, L. L. Bai,

F. M. Zhang, J. Z. Wei and X. J. Sun, *ChemCatChem*, 2019, **11**, 2313-2319.

21. J. Xie, S. A. Shevlin, Q. Ruan, S. J. A. Moniz, Y. Liu, X. Liu, Y. Li, C. C. Lau, Z. X. Guo and J. Tang, *Energy Environ. Sci.*, 2018, **11**, 1617-1624.

22. J. Bi, W. Fang, L. Li, J. Wang, S. Liang, Y. He, M. Liu and L. Wu, *Macromol. Rapid Commun.*, 2015, **36**, 1799-1805.

23. D. Kong, X. Han, J. Xie, Q. Ruan, C. D. Windle, S. Gadipelli, K. Shen, Z. Bai, Z. Guo and J. Tang, *ACS Catal.*, 2019, **9**, 7697-7707.

24. Z. Lin, Y. Wang, Z. Peng, Y. C. Huang, F. Meng, J. L. Chen, C. L. Dong, Q. Zhang, R. Wang, D. Zhao, J. Chen, L. Gu and S. Shen, *Adv. Energy Mater.*, 2022, **12**, 2200716.

25. C. Ye, J.-X. Li, Z.-J. Li, X.-B. Li, X.-B. Fan, L.-P. Zhang, B. Chen, C.-H. Tung and L.-Z. Wu, *ACS Catal.*, 2015, **5**, 6973-6979.

26. J. Zhang, M. Grzelczak, Y. Hou, K. Maeda, K. Domen, X. Fu, M. Antonietti and X. Wang, *Chem. Sci.*, 2012, **3**, 443-446.

27. J. Wang, W. Shi, D. Liu, Z. Zhang, Y. Zhu and D. Wang, *Appl Catal B-Environ*, 2017, **202**, 289-297.

28. S. Chu, Y. Wang, Y. Guo, P. Zhou, H. Yu, L. Luo, F. Kong and Z. Zou, *J. Mater. Chem.*, 2012, **22**, 15519-15521.

29. Z. A. Lan, Y. Fang, Y. Zhang and X. Wang, *Angew. Chem. Int. Ed.*, 2017, **57**, 470-474.